Electronic Supplementary Material (ESI) for Nanoscale
This journal is © The Royal Society of Chemistry 2013

Photovoltaic Enhancement Due to Surface-Plasmon Assisted Visible-Light Absorption at the Inartificial Surface of Lead Zirconate-Titanate Film

Fengang Zheng,[a,b,*] Peng Zhang,[a] Xiaofeng Wang,[a] Wen Huang,[b,c] Jinxing Zhang,[d,e] Mingrong Shen,[a] Wen Dong,[a] Liang Fang,[a] Yongbin Bai,[f] Xiaoqing Shen,[f] Hua Sun[a,*] Jianhua Hao,[b*]

Corresponding authors should be addressed: zhfg@suda.edu.cn;.

This journal is © The Royal Society of Chemistry 2013

Fig. S1. Experimental details and microstructure of PZT film.

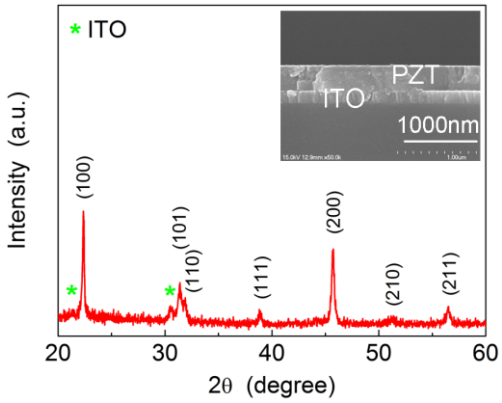

Fig. S1. XRD pattern of PZT film. The inset in Fig. S1 is the cross-section SEM picture of PZT/ITO/quartz sample.

$Pb(Zr_{0.2}Ti_{0.8})TiO_3$ (PZT) film was deposited on ITO coated quartz by sol-gel method, and PZT film was annealed at 600 ^{o}C temperature in oxygen atmosphere (experimental details can be found in our published works[S1,S2]). The crystal structure of PZT film was evaluated by measuring x-ray diffraction (XRD) spectra with Ni filtered CuKα radiation. Scanning electron microscope (SEM) cross-section image was checked by Hitachi S-570. Fig. S1 is the X-ray diffraction (XRD) pattern for PZT film, showing that the PZT film is well-crystallized and has a polycrystalline perovskite structure (JCPDS card No. 70-4260). The inset in Fig. S1 is the scanning electron microscope cross-section image of PZT/ITO/quartz sample. The thicknesses of ITO and PZT layers were 150 and 300 nm, respectively.

Fig. S2. Tunability of photovoltaic by the polarization switching.

Fig. S2 shows the representative photovoltaic current-voltage (PVIV) characteristics of (a) ITO/PZT/Pt, (b) ITO/PZT/Au, (c) ITO/PZT/Cu and (d)

ITO/PZT/Ag structures illuminated under a simulated standard sunlight (AM 1.5G, 100 mW/cm^2). When the photocurrent was recorded, the PZT film was as-grown state (no any poling voltage), remnant polarization up-state (+10 V poling voltage for 5 s) and remnant polarization down-state (-10 V poling voltage for 5 s), respectively.

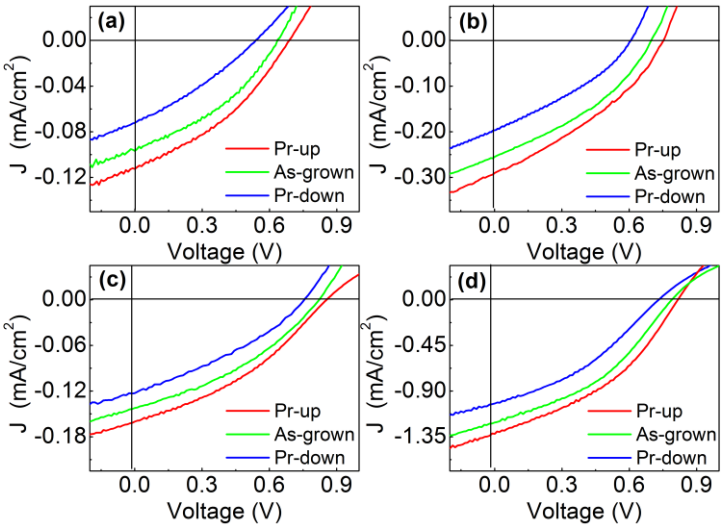

Fig. S2 Photovoltaic current voltage (PVIV) curves of (a) ITO/PZT/Pt, (b) ITO/PZT/Au, (c) ITO/PZT/Cu and (d) ITO/PZT/Ag structures illuminated under a simulated sunlight (100 mW/cm^2, AM1.5G) when PZT film was in as-grown, remnant polarization-down (polarization directs to bottom ITO electrode) and remnant polarization-up states.

When the PZT film is as-grown state, as shown in Fig. S2 (green lines), the photovoltaic output can be mainly attributed to the bottom Schottky barrier ($E_{bi\text{-}bottom}$) at the ITO/PZT interface because the $E_{bi\text{-}bottom}$ is much higher than the top Schottky barrier ($E_{bi\text{-}top}$) at top PZT/metal interface.[S1,S2] Since the $E_{bi\text{-}bottom}$ and $E_{bi\text{-}top}$ is back-to-back and the direction of the $E_{bi\text{-}bottom}$ is pointed to the bottom ITO electrode, the light-induced holes are expelled to the bottom ITO electrode and the light-induced electrons are drifted to the top metal one, subsequently, a positive photocurrent from metal electrodes to ITO can be obtained.[S2] A decrease photocurrent (blue lines in Fig.

This journal is © The Royal Society of Chemistry 2013

S2) can be observed when the PZT film is remnant polarization-down state, in other words, the direction of depolarization field due to the alignment of remnant polarization is opposite to that of the $E_{bi\text{-}bottom}$. On the contrary, an increase photocurrent (red lines in Fig. S2) occurs when the PZT film is remnant polarization-up state.

The photovoltaic parameters, such as V_{OC}, J_{SC}, fill factor (FF) and photoelectric transformation efficiency (η) are listed in Table S1 when PZT film was as-grown state, remnant polarization up-state and remnant polarization down-state, respectively. It is obvious that the photovoltaic output of PZT film is modulated by the polarization switching. If the modulation index of η is defined as $\gamma=(\eta_{max}-\eta_{min})/\eta_{max}$, we can find that the γ is close related to the remnant polarization of PZT film. Here, η_{max} is the η when PZT film is remnant polarization-up state, and η_{min} is the one when PZT film is remnant polarization-down state.

Table S1. Photovoltaic parameters, such as V_{OC}, J_{SC}, FF and η (γ is also listed).

Top electrode		V_{OC} (V)	J_{SC} (mA/cm^2)	FF	η (%)	γ
Pt	As-grown	0.63	0.09	0.39	0.022	0.55
	Polarization-up	0.67	0.11	0.37	0.027	
	Polarization-down	0.54	0.07	0.32	0.012	
Au	As-grown	0.69	0.26	0.36	0.065	0.47
	Polarization-up	0.76	0.29	0.34	0.075	
	Polarization- down	0.60	0.20	0.33	0.040	
Cu	As-grown	0.82	0.14	0.37	0.042	0.39
	Polarization-up	0.85	0.16	0.36	0.049	
	Polarization- down	0.76	0.12	0.33	0.030	
Ag	As-grown	0.78	1.22	0.39	0.37	0.36
	Polarization-up	0.82	1.34	0.38	0.42	
	Polarization- down	0.73	1.03	0.36	0.27	

This journal is © The Royal Society of Chemistry 2013

Fig. S3. Transmissivity spectra of three filters named as K9, JB420 and CB550.

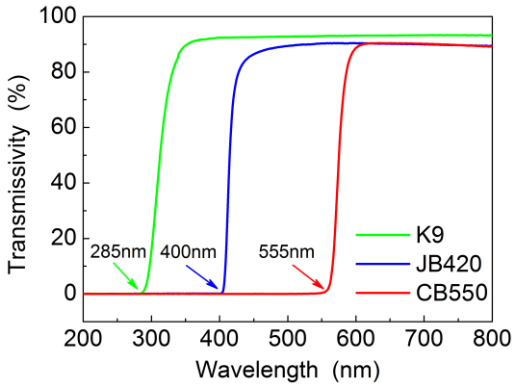

Fig. S3. Transmission spectrum of the filters named by K9, JB400, and CB550.

Fig. S3 shows the transmissivity spectra of three filters named as K9 (green line), JB420 (blue line) and CB550 (red line), respectively. The absorption edges of K9, JB420 and CB550 filters are about 285 nm, 400 nm and 555 nm, respectively. The powers of the transmitted light were 95, 86 and 40 mW/cm^2, respectively, when K9, JB420 and CB550 filters were added in turn between PZT film and a simulated sunlight source (100 mW/cm^2, AM1.5G).

Fig. S4. 2- and 3-dimention AFM pictures of PZT film.

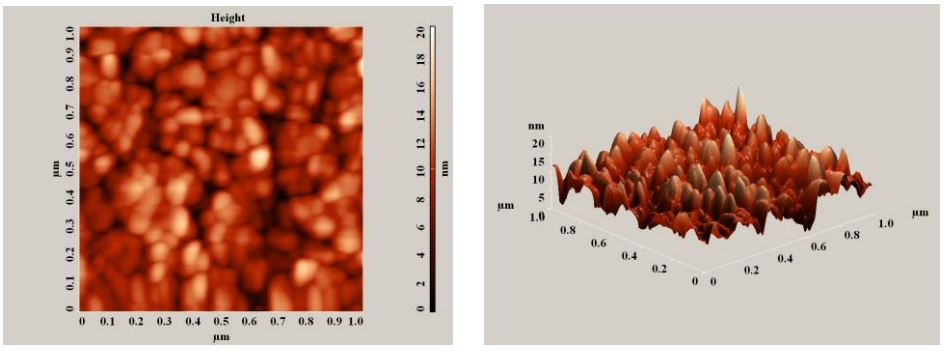

Fig. S4. 2- (left) and 3- (right) dimension AFM picture of PZT film. Scan area is 1×1 μm.

Fig. S4 show the 2- and 3-dimention atomic force microscope (AFM) pictures of PZT film. The grain sizes of PZT film range from 30 nm to 100 nm. From the

This journal is © The Royal Society of Chemistry 2013

3-dimention picture, it can be seen that there are a lot of pyramidal hills on the top surface of PZT film, which formed naturally during the process of annealing at high temperature. The heights of those hills range from 5 nm to 20 nm. It is conceivable that the surface of metal electrode contacted with PZT film may not be completely smooth due to the existing of those hills when the metal electrodes are deposited on the surface of PZT film. We suppose that all the valleys of those hills are stuffed fully by the atoms of metal electrodes, so a rough interface between PZT film and metal electrode is constructed.

Fig. S5. Refractive index and extinction coefficient of PZT film.

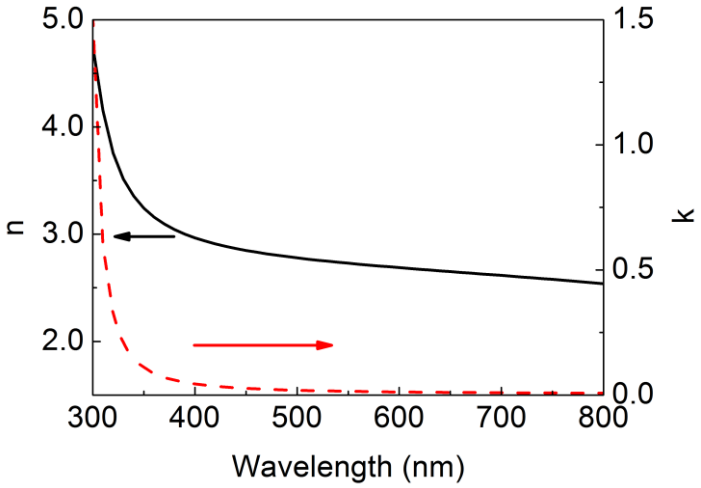

Fig. S5. Wavelength-dependence of the measured refractive index and extinction coefficient of polycrystalline PZT film.

Fig. S6. Absorption for different n of PZT film with Ag electrode.

Fig. S6 shows the resonance peak depends closely on the value of the refractive index of PZT (n). A significant blue shift of the resonance peak is observed when the

This journal is © The Royal Society of Chemistry 2013

PZT refractive index is lowered from the values n_0 of the whole PZT film. Particularly for n= n_0-0.4, the SP resonance occurs in the range from 420nm to 520nm, consistent with the visible-range part of the measured EQE enhancement. Note that after the correction n= n_0-0.4, the refractive index of PZT near the interface is about 2.276 at 615nm, which agrees with the fitted value 2.263 of the refractive index of the PZT region close to the surface of Au nanoparticles in Ref. S3.

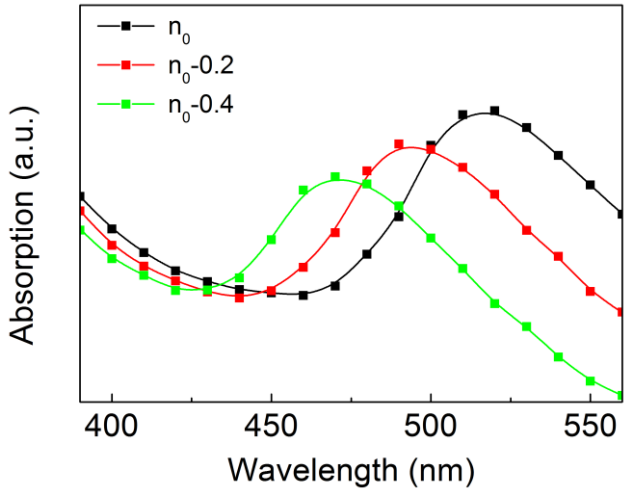

Fig. S6. Absorption in the Ag electrode with rough surface for different refractive index of PZT film. n_0 is the measured values for the whole PZT film.

Fig. S7. Absorption blue shift for a low refractive index of PZT film with Au electrode.

A similar blue shift of the resonance peak is observed when the PZT refractive index is lowered from the values n_0 of the whole PZT film. Good agreement between the calculations and experiments can also be found for the same corrected refractive index of PZT when the Au electrode is employed, where the calculated resonance region is across 520nm-700nm with a peak around 570nm as shown in Fig. S7.

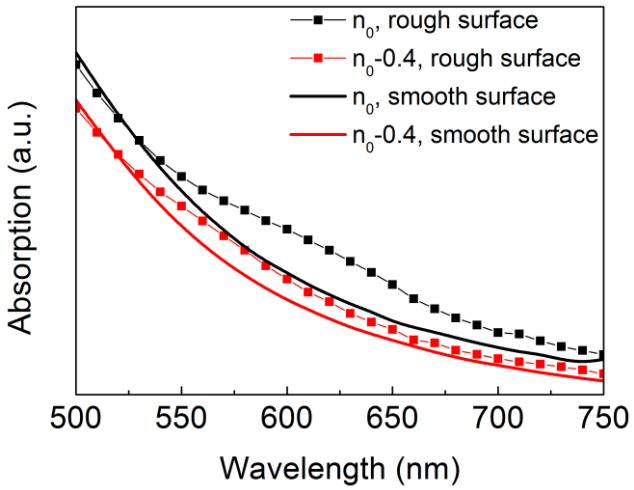

Fig. S7. Blue shift of the SPR peak of the Au electrode when the refractive index of PZT is corrected as n= n_0-0.4

Fig. S8. Effect of annealing at 500 ℃ on other three devices.

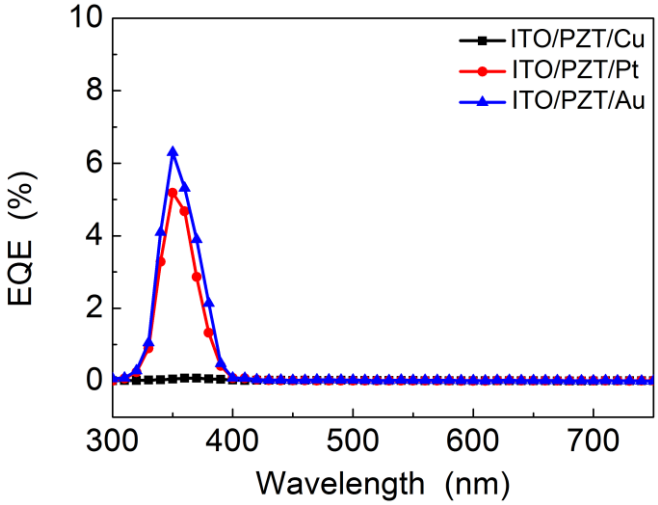

Fig. S8 Effect of annealing at 500 ℃ on ITO/PZT/Cu, ITO/PZT/Pt and ITO/PZT/Au structures.

Fig. S8 shows the effect of annealing at 500 ℃ on ITO/PZT/Cu, ITO/PZT/Pt and ITO/PZT/Au structures. After ITO/PZT/Cu sample was annealed at 500 ℃, Cu electrode has been oxidized as CuO material (black color) with a poor conductivity, resulting in a very tiny photocurrent that cannot almost been observed. When Pt electrode was annealed at 500 ℃, the height of Schottky barrier at the PZT/Pt

interface increased to about 0.64 eV.[S4] Because top and bottom Schottky barriers are back-to-back, this increasing top Schottky barrier can lead to a decreasing deference between bottom Schottky barrier and top one, as a results, the EQE data decrease. A similar phenomenon was observed in ITO/PZT/Au structure, where the height of Schottky barrier at the PZT/Au interface was lower about 0.1 eV than that at the PZT/Pt interface.[S5]

Fig. S9. Fields and light-induced charges in the PZT film.

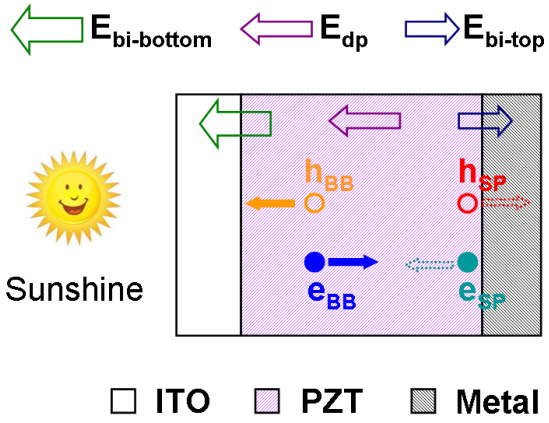

Fig. S9. Diagram of fields in the PZT film (remnant polarization-up state). h_{BB} and e_{BB} are the UV light-induced hole and electron due to the band-to-band absorption in the PZT film, respectively. h_{SP} and e_{SP} are the visible light-induced hole and electron due to the SP at the surface of PZT film, respectively.

As shown in Fig. S9, if the $E_{bi\text{-}top}$ is assumed to be zero, h_{SP} can be drifted to the bottom ITO electrode (at the same time, e_{SP} are moved to the top metal electrode), which is the same as the transport of h_{BB} and e_{BB} drifted by the $E_{bi\text{-}bottom}$ and the E_{dp} (the action of E_{dp} is far smaller that that of the $E_{bi\text{-}bottom}$, as shown in Fig. S2). Because the $E_{bi\text{-}bottom}$ was far larger than the $E_{bi\text{-}top}$ before the top metal electrode is annealed, a

This journal is © The Royal Society of Chemistry 2013

part of h_{SP} (e_{SP}) can be drifted to the bottom ITO (metal) electrode. After the top electrode is annealed, the top $E_{bi\text{-}top}$ is enhanced. A great part of h_{SP} is moved to top metal (at the same time, e_{SP} to the ITO electrode), as shown in Fig. S9, which direction is opposite to that of the photocurrent due to the h_{BB} and e_{BB}. Here, the photocurrent due to the SP can be cancelled out by the photocurrent due to the band-to-band absorption.

If we suppose the $E_{bi\text{-}bottom}$ is equal to zero, the photocurrent is determined completely by the Schottky barrier of top PZT/metal interface, which is similar to the issue of TiO_2/Au (or Ag) SP system.[S6,S7] From Fig. S9, we can conclude that the high Schottky barrier is helpful to enhance the photocurrent due to SPs at the semiconductor/metal interface, which is not contradictory to the conclusion widely accepted in the TiO_2/Au (or Ag) SP system.

References:

S1 D. W. Cao, C. Y. Wang, F. G. Zheng, W. Dong, L. Fang, M. R. Shen, *Nano Lett.*, 2012, **12**, 2803.

S2 P. Zhang, D. W. Cao, C. Y. Wang, M. R. Shen, X. D. Su, L. Fang, W. Dong and F. G. Zheng, *Mater. Chem. and Phys.*, 2012, **135**, 304.

S3 K. C. Hsieh, H. L. Chen, D. H. Wan and J. Shieh, *J. Phys. Chem. C*, 2008, **112**, 11673.

S4 D. W. Cao, H. Zhang, L. Fang, W. Dong, F. G. Zheng and M. R. Shen, *Appl. Phys. Lett.*, 2010, **97**, 102104.

This journal is © The Royal Society of Chemistry 2013

S5 M. Qin, K. Yao, Y. C. Liang and B. K. Gan, *Appl. Phys. Lett.*, 2007, **91**, 092904.

S6 Z. H. Zhang, L. B. Zhang, M. N. Hedhili, H. N. Zhang and P. Wang, *Nano Lett.*, 2013, **13**, 14.

S7 H. Y. Li, W. B. Lu, J. Q. Tian, Y. L. Luo, A. M. Asiri, A. O. Al-Youbi and X. P. Sun, *Chem. Eur. J.*, 2012, **18**, 8508.